Spectral Properties of Accretion Disks Around Black Holes II – Sub-Keplerian Flows With and Without Shocks[1]

Sandip K. Chakrabarti[2]
S.N. Bose National Center for Basic Sciences JD Block, Sector III, Salt Lake, Calcutta 700091, India
and
Tata Institute of Fundamental Research, Mumbai, 400005, India
e-mail: chakraba@tifrc2.tifr.res.in

ABSTRACT

Close to a black hole, the density of the sub-Keplerian accreting matter becomes higher compared to a spherical flow due to the presence of a centrifugal barrier independent of whether or not a standing shock actually forms. This hot dense flow intercepts soft photons from a cold Keplerian disk and reprocesses them to form high energy X-rays and gamma rays. We study the spectral properties of various models of accretion disks where a Keplerian disk on the equatorial plane may or may not be flanked by a sub-Keplerian disk and the sub-Keplerian flow may or may not possess standing shocks. From comparison with the spectra, we believe that the observed properties could be explained better when both the components (Keplerian and sub-Keplerian) are simultaneously present close to a black hole, even though the sub-Keplerian halo component may have been produced out of the Keplerian disk itself at larger radii. We are able to understand soft and hard states of black hole candidates, properties of X-ray novae outbursts, and quasi-periodic oscillations of black hole candidates using these two component models. We fit spectra of X-ray novae GS1124-68 and GS2000+25 and satisfactorily reproduce the light curves of these objects.

Subject headings: accretion, accretion disks – black hole physics – radiation mechanisms: nonthermal – shock waves – stars: neutron

---

[1]Submitted:11th Nov. 1996; Accepted: Jan. 22 1997; Astrophysical Journal (in press)

[2]On leave from TIFR, Mumbai 400005, India

1. INTRODUCTION

Recently, Chakrabarti & Titarchuk (1995, hereafter referred to as Paper I) proposed that in order to understand the soft and hard states of black hole candidates, one need not look for any elusive 'Compton cloud' or any so-called magnetized corona. One can satisfactorily explain all the major quasi-steady properties of black hole candidates by a two component accretion flow model (TCAFM). Based on analytical solutions of generalized accretion disk models (Chakrabarti, 1990; Chakrabarti & Molteni, 1995; Chakrabarti 1996a, hereafter C96a) they showed that an accretion disk should naturally segregate into two regions, one a Keplerian disk on the equatorial plane and the other a sub-Keplerian halo flanking the Keplerian disk, although eventually the Keplerian component should also become sub-Keplerian close to the black hole in order to satisfy boundary conditions on the horizon. The sub-Keplerian halo is hot, optically thin, and faces a centrifugal barrier close to the black hole; as a result, its density increases much faster than that of a spherical Bondi flow. This 'puffed up' optically thin gas located just outside the horizon may intercept soft photons coming from the cooler Keplerian disk and re-emit them as photons of higher energy (hard X-rays and gamma-rays in the case of galactic black hole candidates, and UV and soft X-rays in the case of massive black hole candidates). Detailed study of the behavior of the sub-Keplerian component (Chakrabarti 1989, hereafter C89; C96a) shows that in a considerable region of the parameter space, the flow actually forms a standing shock where the density and temperature rise abruptly. In the case of the formation of *strong* shocks (where density jumps by a factor of four) the electron number density is high in the post-shock region, and Paper I shows that the accretion rate of the Keplerian disk where a hard state (typically, when the energy spectral index $\alpha \sim 0.5 - 0.8$) to a soft state (typically, when the energy spectral index $\alpha \sim 1.3 - 1.8$) transition takes place is around $0.1 - 0.3\dot{M}_{Edd}$ (where $\dot{M}_{Edd}$ is the Eddington rate), depending on the accretion rate of the sub-Keplerian component. In the future, we shall call this model as TCAFM1.

However, in the general classification of C89 and Chakrabarti (1996b, hereafter C96b), the rest of the parameter space does not allow the formation of standing shocks. The density and temperature enhancements are gradual, though ultimately achieving values close to the hole similar to those of the post-shock flows (C96a and Chakrabarti, 1997 hereafter C97). We discuss the nature of these regions below as well. Existence of these solutions enables us to explore other possible models which we carry out in the present paper. These models are: (a) TCAFM2 – Here the shock is weak or absent altogether, but the flow feels a centrifugal barrier due to the angular momentum. (b) TCAFM3 – Here the sub-Keplerian component does not have any angular momentum, and is basically a spherical inflow. This case is considered to bring out the important fact that the observed properties of black hole candidates may definitely require some angular momentum. And finally, (c) SCAFM, Single Component Accretion Flow Model – Here the sub-Keplerian halo is completely non-existent, and only the Keplerian component becomes sub-Keplerian close to the black hole. It is to be noted that another single component (inviscid) solution is possible where the flow remains fully sub-Keplerian and the post-shock flow (with or

without shocks) intercepts soft-photons from the pre-shock region. This has been studied by Chakrabarti & Wiita (1992) in the context of spectra of active galaxies and quasars.

In this context we differentiate two types of black holes candidates depending on the time scales in which their states are changed. If the candidate is an X-ray nova, then it may be repeated in a very long time scale (several tens of years, say). This time scale is probably dictated by the limit cycle behavior (Cannizzo, 1993) in which the viscosity at the outer edge of the Keplerian disk rises and falls periodically and the mass accretion rates also can change. In the quiescent states, with low accretion rate, the hot flow accretes basically as a sub-Keplerian disk since the deviation from a Keplerian disk takes place very far away from a black hole ($X_K >> 1$, Paper I, C96). During the rising phase of a nova outburst, the hard X-ray brightens in a matter of a few $(2-5)$ days which may correspond to the viscous (upper branch of the limit cycle) time scale in which Keplerian disk component rapidly comes closer to the black hole. Keeping this in mind, we also study a variation of TCAFM2 and TCAFM3 models (called TCAFM2_2 and TCAFM3_2 respectively) in which the transition radius X_K is varied in a viscous time scale. In the decaying phase of a nova, both the accretion rates as well as X_K (where deviation from a Keplerian disk takes place) are expected to change in an as yet poorly understood manner. Nevertheless, the soft to hard transition could be understood generally in terms of the relative abundance of Keplerian and non-Keplerian matter, as we show below. In the case of otherwise inactive black holes (e.g., away from novae activities), the soft state to hard state (and vice versa) may take place several times in a matter of days or months. These cases could be due to variation of viscosity in these time scales and the Keplerian and sub-Keplerian components could be re-distributing their rates accordingly, while maintaining the sum of the rates roughly constant. Keeping these systems in mind, we study a model (TCAFM1_2) where the sum of the rates are kept fixed.

The current Paper is organized as follows: In the next Section, we classify all the solutions in thin accretion flows. Using this as the reference point, we discuss our disk models and the way the spectra are computed. In §3, we present solutions of various models. In §4, we compare solutions of our models with observations of X-ray novae. Finally, in §5, we present our conclusions.

2. DISK MODELS

In Fig. 1, we classify the *entire* parameter space according to the type of solutions of thin inviscid flow that are prevalent around a Schwarzschild black hole. Here we use two conserved parameters, namely, specific energy $\mathcal{E}$ and specific angular momentum l for classification (as opposed to, say, entropy accretion rate $\dot{\mathcal{M}}$ and l as used in 1.5D flow in C89). The adiabatic index $\gamma = 4/3$ has been chosen. The whole space is divided into nine regions marked by N, O, NSA, SA, SW, NSW, I, O^*, I^*. The horizontal line at $\mathcal{E} = 0$ corresponds to the rest mass of the flow.

The parameters from region N do not produce any transonic solution. The solutions from the region 'O', which have very low angular momentum and energy are similar to a Bondi flow and

have only the outer sonic point. The solutions from the regions NSA and SA have two 'X' type sonic points with the entropy density S_o at the outer sonic point *less* than the entropy density S_i at the inner sonic point. However, flows from SA pass through a standing shock since the Rankine-Hugoniot condition is satisfied. The entropy generated at the shock, $S_i - S_o$, is advected towards the black hole to enable the flow to pass through the inner sonic point. Rankine-Hugoniot condition is not satisfied for flows around a black hole from the region NSA. However, for flows around a neutron star the shock condition is satisfied right outside the star surface (C89). Numerical simulations show (Ryu, Chakrabarti & Molteni, 1997) that the flow from this region could be very unstable and could exhibit periodic changes in emission properties as the flow constantly tries to form the shock wave, but fails to do so. These solutions explain quasiperiodic oscillations very satisfactorily.

The solutions from the regions SW and NSW are very similar to those from SA and NSA. However, $S_o \geq S_i$ in these cases. Shocks can form only in winds from the region SW. The shock condition is not satisfied in winds from the region NSW even though two sonic points are present. This may make the NSW flow unstable as well. A flow from region I only has the inner sonic point and thus can form shocks (which require the presence of two saddle type sonic points) only if the inflow is already supersonic due to some other physical processes (such as flaring of the inflow, or capturing of companion winds; see, C90, C97). Each solution from regions I^* and O^* has two sonic points (one 'X' and one 'O') only but none produces any complete and global solution. The region I^* has an inner sonic point but the solution does not extend subsonically to a large distance. The region O^* has an outer sonic point, but the solution does not extend supersonically to the horizon. When a significant viscosity is added, the closed topologies of I^* and O^* open up as described in C90ab and C96, and the flow may join with a cool Keplerian disk with $\mathcal{E} < 0$. These special solutions of viscous transonic flows need not have centrifugally supported shock waves as they have only one inner sonic point. However, hot flows deviating from a Keplerian disk, or sub-Keplerian winds from companions, or cool flows subsequently energized by magnetic flares (for instance) will have $\mathcal{E} > 0$, and thus could have standing or periodically varying shock waves as discussed above. The post-shock region or the enhanced density region radiates most of the observed hard radiation. The present classification is done using thin flows in the Paczyński–Wiita (1980) potential. A similar division of parameter space in the Kerr geometry is presented elsewhere (Chakrabarti, 1996c).

In Paper I, we have already discussed in detail the nature of the two component hydrodynamical model. In the present paper, in view of the classification described above, we not only study that model, we also assume that the shock need not be always strong as was assumed in Paper I, or need not always be present. Fig. 2 shows schematically the general nature of the multi-component accretion flows. If the basic assumption that the viscosity falls off with height is correct, then when the accretion rate in the sub-Keplerian component is low, then the lowest viscosity region separates out (at X_{K2}) as a giant big thick disk (of size $\sim 10^4 R_g$) while the intermediate viscosity region separates out (at X_{K1}) as a sub-Keplerian flow which may or may

not have a shock wave (at X_S). If the shock does not form then $X_S \sim X_{K1}$ and $X < X_S$ is simply the centrifugal barrier supported dense region which reprocesses the soft photons in the same way as the post-shock region of Paper I. In the hard state, the giant (geometrically) thick disk (which is like an extended atmosphere of optical depth of the order unity) reprocesses the hard and soft radiations and may even remove the soft bump altogether (as seen in Cyg X-1, see, Kazanas, Hua & Titarchuk, 1997). When the viscosity is increased and the Keplerian accretion rate is increased, the giant thick disk also collapses (this can be understood from the Fig. 10 of Paper I) thereby exposing the Keplerian disk along with the cool post-shock region to the observer.

In the case when the angular momentum of the sub-Keplerian component is negligible (TCAFM3), the Keplerian disk is simply assumed to be 'embedded' in a wedge-shaped infalling 'Bondi' cloud which changes its conical thickness at the place where the Keplerian disk also becomes sub-Keplerian. At this place, the thickness (which determines the fraction of soft-photons intercepted by the cloud) is computed from the average local temperature of the gas, which is roughly the same as that when the shock is present. The actual thickness and interception may depend on details, but the conclusion from this model does not. In the case where shocks are not present or are weak (TCAFM2), the density is increased due to the centrifugal barrier as matter comes closer to the black hole. The detailed solution of the governing equations (e.g., Fig. 7a of C96a, and Fig. 3 of C97) shows that independent of whether a shock is present or not, for a given angular momentum at the inner edge of the disk, the flow has roughly the same distribution of velocity and density, though in the presence of shocks this variation is more abrupt. In the Single Component Accretion Flow Model (SCAFM), the sub-Keplerian halo component is not assumed to be present at all. The Keplerian disk becomes sub-Keplerian at X_K, and the density thereon was computed using the standard procedure with the angular momentum barrier taken into account as in TCAFM2. As will be shown below, this case always tends to produce soft states.

In the models TCAFM2_2 and TCAFM3_2, the location X_K is varied and the corresponding spectra are computed. Generally speaking, in the presence of a steady sub-Keplerian component, the object should go from a hard state to a soft state as X_K becomes smaller (due to variation of viscosity for example, see, C90, Paper I, C96ab) and more and more soft photons are intercepted by the sub-Keplerian enhanced density region close to the black hole. In the rising phase of novae outbursts such a process may indeed be taking place on viscous time scales dictated by the higher value of viscosity during the limit cycle, while in the decaying phase of novae outbursts such a process may take place in a reverse order, on time scales dictated by the smaller viscosity during this phase of the limit cycle. This is suggested by the fact that viscosities in the two branches are off by almost two orders and the rise time scale of a novae outburst is also about two orders of magnitude shorter compared to the decaying time scale. Of course, the effect due to varying X_K is superimposed on the (exponentially or linearly, as the case may be) decaying mass accretion rates, as discussed in §4 below.

In all the model calculations, we assume the mass of the black hole to be $1 M_\odot$. This is uncorrected for the spectral hardening (Shimura & Takahara, 1995) factor f as in Paper I. Thus,

assuming $f \sim 1.9$, our solutions here are valid for a black hole of mass $f^2 M_\odot \sim 3.6 M_\odot$. The general results are valid even for supermassive black holes in a trivial way, since the electron temperature in the enhanced-density-region (which serves as the electron cloud in our model) is very insensitive to the black hole mass. (In fact the virial temperature is independent of the black hole mass, but considering corrections due to cooler disk photon temperatures, we find empirically that the electron temperature varies as $T_e \sim M_{BH}^{0.04-0.1}$, keeping all other non-dimensional inputs same.). The spectra are computed assuming a line of sight angle of $\sim 37^\circ$ (cos $i = 0.8$). The accretion rates are always quoted in units of the Eddington rate, and the distances are measured in units of the Schwarzschild radius $R_g = 2GM_{BH}/c^2$. In some of the cases the effect of bulk motion Comptonization (Paper I and references therein; Ebisawa, Titarchuk & Chakrabarti 1996) has been added just for comparison.

3. SPECTRAL PROPERTIES OF DIFFERENT ACCRETION FLOW MODELS

To remind the readers, we describe the procedure of computation of the spectra here, but details are in Paper I. We generally assume two accretion rates, $\dot{m}_d$, the rate of the Keplerian component, and $\dot{m}_h$, the rate of the sub-Keplerian halo component. It is to be noted that these two independent rates obviates the need to use one single rate (sum of Keplerian and sub-Keplerian) and an unknown viscosity parameter. However, depending on astrophysical circumstances, the sum of the two rates may or may not be constant with time (as discussed in the Introduction). Once $\dot{m}_d$ is assumed, the zeroth order temperature distribution of the Keplerian disk is computed from a standard Shakura-Sunyaev (1973) disk. Similarly, once the $\dot{m}_h$ is chosen, the density distribution is computed from a standard hydrodynamical model (Paper I) and the temperature is computed using a two-temperature disk model with bremsstrahlung, Comptonization, proton-electron Coulomb coupling, inverse bremsstrahlung, etc. The matter from both components are mixed below X_K ($= X_s$ if shocks are present). The electron temperature in the sub-Keplerian inner region below X_K is computed and then averaged using the prescription given in Paper I and the spectral index is computed using standard procedures (Sunyaev & Titarchuk, 1985; Titarchuk 1994). The feedback from the sub-Keplerian cloud onto the cooler Keplerian disk is computed using the proper albedo (Paper I) and the spectral index is recomputed using the modified cool disk temperature. The procedure is iterated until the spectral index, the disk temperature distribution, and the electron temperature all converge.

3.1. When a Strong Shock is Present

In this case we study the model TCAFM1. Fig. 3 shows the nature of the spectra. Here, we choose $\dot{m}_h = 1$ and $\dot{m}_d = 1,\ 0.1,\ 0.01,\ 0.001,\ 0.0001$ as marked. The shock location is chosen at $X_s = 10$, which is the most likely place in a Schwarzschild geometry (Paper 1). The inner edge is chosen at $X_i = 3$, but the spectra from thermal Comptonization alone depend weakly on the exact

location as the surface area of this region goes down rapidly. In this model, the system goes from hard state to the soft state when the accretion rate of the Keplerian component is increased. The variation of the spectral index will be presented in §3.5. The dotted curve is drawn incorporating consideration of the bulk motion Comptonization (Paper I), which produces a weak hard tail even in the soft state.

Occasionally, the net accretion rate of the inflow may remain constant and the internal variation of viscosity would simply re-distribute Keplerian and sub-Keplerian components differently, as discussed in Paper I. This is our TCAFM1_2 model. Fig. 4a depicts the spectral variation for one such case where the sum is kept at twice the Eddington accretion rate ($\dot{m}_d + \dot{m}_h = 2$). The curves are drawn for various Keplerian disk rates as marked. In this case, the gravitational potential energies of matter are released in soft and hard components at different rates, depending on the availability of soft photons in the Keplerian disk. The net energy released is roughly constant, as is observed in many black hole candidates (Zhang et al., 1997). The pivoting property is also seen to be present. The shock location is assumed to be $X_s = 10$ here. By increasing X_s, the pivoting energy could be reduced. (Typical variations of X_s with angular momentum in a vertically averaged model of the flow are presented in C89.) The effect of the bulk motion Comptonization for the case $\dot{m}_d = 1$ is also shown in dotted curves. In Fig. 4b, we present the variation of the mean electron temperature of the sub-Keplerian cloud close to the black hole with the disk accretion rate (spectral index variation will be presented in §3.5). Here, the electron temperature goes down as the Keplerian rate goes up. The solid curve shows the variation keeping the halo rate fixed (the case corresponding to Fig. 3 of TCAFM1) and the dashed curve shows the variation keeping the sum of the rates fixed (the case corresponding to Fig. 4a of TCAFM1_2). We note that in the latter case, the mean electron temperature is generally constant (around $100 - 150$keV) in the hard state, while at about $\dot{m}_h \sim 0.3 - 1$, the temperature goes down to a few keV rather catastrophically and the object reaches the soft state. In fact, given that the efficiency of extraction of energy from the sub-Keplerian component is less than what is allowed from the conversion of the gravitational potential energy, it is likely that the halo rate actually increases much faster than what is dictated by merely keeping the sum constant. This is probably supported by observed rigorous constancy of the spectral index in each state.

3.2. When the Sub-Keplerian Component has no Angular Momentum

This model is TCAFM3. Figure 5 shows the spectral variation with the Keplerian disk accretion rate $\dot{m}_d$ (as marked) while the halo rate $\dot{m}_h$ is chosen to be unity as before. In this case, the absence of angular momentum reduced the electron density of the sub-Keplerian Compton cloud at the inner edge. Therefore, for a given halo rate, the hard X-ray emission is lower as can be seen by comparing with Fig. 3. Furthermore, it takes fewer soft photons (namely, smaller $\dot{m}_d$) in order to bring the system to soft state, as is clear from the spectra. The actual comparison of the spectral indices is done in §3.5. The effect of bulk motion Comptonization is similar as in the

earlier models and is not shown.

In this particular Model, it is instructive to study the variation of spectral index when the transition radius X_K (where the disk deviates from a Keplerian disk) is varied. This is our TCAFM3$_2$. In presence of low angular momentum flow, viscosity influences the distribution very strongly and X_K decreases with the increase of viscosity (for a given inflow angular momentum on the horizon). In Fig. 6a the results are shown. As X_K is monotonically decreased, the black hole goes from hard to soft state. The halo rate is kept fixed at $\dot{m}_h = 1$ and the Keplerian rate is fixed at $\dot{m}_d = 0.05$. It is to be contrasted with the case when the sub-Keplerian halo is absent where the disk always remains in a soft state (see below). In Fig. 6b, we show how the spectral index is changed as the transition radius X_K is reduced. A possible variation of this model is obtained where the Keplerian disk is originally situated very far away ($\sim 10^4$) as in a low viscosity, low accretion rate, disk (see, Fig. 2a of C96a) and then it approaches the black hole as viscosity is enhanced. In this case, the object, though very faint, has the signature of a soft state. But as the viscosity starts increasing and X_K starts getting smaller, the disk first becomes very bright in hard X-ray and then goes back to the soft state once more with fainter hard X-ray. This type of behavior is common in novae outbursts (Ebisawa et al. 1994; Kitamoto et al. 1992). In Fig. 7a-b, we show the spectral variation in this case. Values of X_K are marked on the curves. We fix $\dot{m}_h = 1$ for illustration purposes. In Fig. 7a, we choose $\dot{m}_d = 0.001$, and in Fig. 7b, we choose $\dot{m}_d = 0.01$. In reality, both rates should increase with time when the rising phase of an X-ray outburst is considered. The spectral index variation in this case will be shown in §3.4. Note that in Fig. 7a, the spectra remains basically in hard states, since the intercepted photon number is too small compared to the electron density. In Fig. 7b, the Keplerian rate is 10 times higher, and as a result, the flow goes to the soft state as X_K decreases to around $X_K \sim 30$.

3.3. When the Shock is Weak or Absent

Here, angular momentum is present but the shock conditions are not satisfied. This is our model TCAFM2. Fig. 8 shows the variation of the spectral index with $X_K = 10$ and $\dot{m}_h = 1$. The hard to soft state transitions take place due to an increase in the number of soft photons relative to the electron numbers as before; the soft photon numbers are characterized by the disk accretion rates $\dot{m}_d$ indicated on the curves. The result is very similar to TCAFM1, where a strong shock is present. This is because the density variation in the post-shock region is similar to the density variation in the centrifugal barrier for the same value of angular momentum (which is chosen to be 1.837, the marginally stable value, in the present run). The variation of the spectral index with $\dot{m}_d$ is shown in §3.5.

As in the previous sub-section, it may be instructive to study the spectral properties when the transition radius X_K is varied. This corresponds to TCAFM2$_2$ model. Fig. 9 shows the results with X_K marked on the curves. The accretion rates are the same as used in drawing Fig. 7b above. Note that in the beginning, the hard X-ray intensity is brightest and the soft component is

weakest. As the viscosity of the flow is increased and the transition radius is reduced, the object becomes softer. This case and that presented in Fig. 10b may be suggestive of why the X-ray novae appear brightest first in the hard X-rays and then become brighter in the soft X-rays. In reality, clearly, after the transition radius of around $X_K = 10$ is reached, the soft X-ray bump continues to rise because of the increase in $\dot{m}_d$ due to enhanced viscosity. The variation of the spectral index in this model is compared with other models in §3.4.

3.4. When the Sub-Keplerian Component is Absent

For the sake of argument, we assume that the sub-Keplerian component does not exist, namely, that the disk is originally fully Keplerian and subsequently totally becomes sub-Keplerian at X_K. We show below that we always obtain a soft state. This is our Single Component Accretion Flow Model (or, SCAFM). This final exercise is to demonstrate the importance of having separate 'electron fuel' in the form of a sub-Keplerian, inefficiently radiating flow along with the Keplerian disk, as assumed in all the models presented above. A similar variation as in the previous sub-section could be studied by changing X_K as is believed to be induced by viscosity (we call this as SCAFM$_2$). The results with $\dot{m}_d = 0.01$ are shown in Fig. 10a where we mark the respective X_K values identifying each curve. Note that the flow is always in the soft state, but since the flow rate is very small, the bulk motion Comptonization is negligible as well and the weak hard tail of slope ~ 1.5 that is seen in soft states cannot be produced in this model. This vindicates our claim that the sub-Keplerian component is essential to supply an extra set of hot electrons. In Fig. 10b, we present the spectral index variation with X_K (long-dashed curve). For comparison, we plot the same quantity for TCAFM3$_2$ (short-dashed curve) and TCAFM2$_2$ (solid curve) models. As noted above, SCAFM$_2$ always produces a soft state even when the disk rate is very low. What is interesting, however, is that the spectral index shows a distinct minimum. This is because when X_K is very large, the electron density in the sub-Keplerian region near the transition radius X_K is very small and they can be cooled even by a small number of soft photons. Similarly, when X_K is very small, the number of soft photons is very high and can easily cool the sub-Keplerian flow. Due to the extra sub-Keplerian component ($\dot{m}_h \neq 0$) in the two component models, the electrons are not easily cooled by a few soft photons from the Keplerian disk. Thus, they tend to produce harder states, except when the Keplerian disk comes too close to the black hole. In the present Figure, we use two cases for TCAFM2$_2$ (marked): $\dot{m}_d = 0.01$ and 0.001 for comparison. For $\dot{m}_d = 0.001$ the photons are always too few to produce soft states. For $\dot{m}_d = 0.01$ the soft state is produced when X_K is small enough, $\sim 50 - 60$ (see also, e.g., Fig. 6[a-b] for $\dot{m}_d = 0.05$). Results of TCAFM3$_2$ is drawn for $\dot{m}_d = 0.01$.

3.5. Comparison of Model Spectra

To understand differences among the models we plot the spectra of all the three models, TCAFM(1-3) in Fig. 11a and the spectral indices in Fig. 11b. The solid, long-dashed and short-dashed curves are for TCAFM1, TCAFM2 and TCAFM3 respectively. Three sets of curves are drawn for Keplerian component rates $\dot{m}_d = 0.3,\ 0.05,\ 0.0005$ and the halo rate is fixed at $\dot{m}_h = 1$, and $X_K = 10$ ($= X_s$ for TCAFM1). The solution including shocks is the hardest, since for a given set of accretion rates, the opacity is highest in the enhanced density region when a strong shock is present. This is reflected in the spectral index variation as well. For comparison, we present also the spectral index variation in the TCAFM1_2 model where the *sum* of the accretion rates is kept fixed. This is shown as the (lower) short-dash-dotted curve in Fig. 11b. Note that it has the most pleasant feature of having almost constant spectral index even when $\dot{m}_d$ is increased by a factor of a thousand. We have plotted the case where $\dot{m}_{sum} = \dot{m}_d + \dot{m}_h = 2.0$ and hence the spectral index is on the low side ($\sim 0.4 - 0.5$) in the hard state. For a smaller $\dot{m}_{sum} = 1$ the index is higher (the upper short-dash-dotted curve). All the models definitely bring the system to a soft state much before the Eddington rate is approached. It is clear that the Keplerian rate where the soft state is produced depends on opacity, which in turn depends on the sum of both the Keplerian and the sub-Keplerian accretion rates and the model of the flow, i.e., whether the centrifugal barrier is present or not.

As discussed in Paper I, when the accretion rate is very high, the electrons in the sub-Keplerian region are totally cooled off to a few keV (see, Fig. 4b above). However, they can still be energized to several hundreds of keV by the so-called bulk motion Comptonization where the relativistically moving electrons directly transfer their momentum to the trapped soft photons. The resulting spectral index is ~ 1.5 which is observed in the soft states of most of the black hole candidates (Ebisawa et al. 1996). The variation of the spectral index with $\dot{m}_d$ (when $\dot{m}_h = 1$ is chosen) is shown in solid curve on the right part of Fig. 11b. Note that there is a considerable overlap between the Comptonization processes near $\dot{m}_d \sim 1$. Here, the power-law component should be contributed by both the Comptonization processes and thus a break in power law is expected. This may also have been seen in Cyg X-1 (Zhang et al. 1997). The long-dash-dotted curve drawn in this region assumes the presence of strong shock (where the density goes up by a factor of four for a given accretion rate). As a result, the slope of 1.5 is achieved at a much lower disk accretion rate that that obtained from a spherical convergent flow (solid curve). Accretion rates obtained from observations probably agree with the results obtained using this enhanced density region (long-dash-dotted curve).

4. COMPARISON WITH OBSERVATIONS OF X-RAY NOVAE

It is interesting to compare the results of the two component accretion flow models presented above with some of the observations of black hole candidates. In Fig. 12 spectral evolutions of

two well known X-ray novae are qualitatively fitted with results of TCAFM1. The spectral data of GS2000+25 are taken from Tanaka (1991) and those of GS1124-68 are from Ebisawa (private communication, 1996; Ebisawa et al., 1994). For simplicity and to highlight the similarity between these two objects, all the parameters have been kept fixed (with $X_s = 10$ and Schwarzschild black hole of mass $1M_\odot$ which after correction due to spectral hardening corresponds to $3.6M_\odot$) *except* for the rates $\dot{m}_d$ and $\dot{m}_h$. Figs. 12(a-b) show these fits. From the derived pair of rates ($\dot{m}_d$, $\dot{m}_h$) the intermediate rates are interpolated and the resulting light curves ($1 - 20$keV) are shown in Figs. 12(c-d). Solid and dotted light curves are respectively drawn using linear-linear and linear-log interpolations of $\dot{m}_d$. In Fig. 12(c), squared points are obtained from the actual spectra while crosses are obtained from the fit in Fig. 12(a). In Fig. 12(d), the squares are from ASM light curve of Ginga (Kitamoto, private communication, 1996; Kitamoto et al. 1992). The general features of the light curves are clearly reproduced, including the bumps after $50 - 70$ days and another one after 200 days of outburst. Both show a decay time scale of ~ 33 days. The bump around $50 - 70$ days shows that the decay of disk accretion rate is not really exponential, but closer to linear, although after around 200 days the disk accretion rate has dropped to the point where the exponential decay would have brought it anyway. This temporary deviation from exponential decay is suggestive of a major change in flow topology, which may occur as the viscosity crosses the critical values (C90, C96a). For very low and very high viscosities the flow may pass only through the inner sonic point, while for intermediate viscosities the flow may have to pass through only the outer sonic point unless shocks also form (see, Fig. 2a of C96a). The rising light curves in both the cases were computed in two different ways and the results were similar. In one case (using TCAFM1), the $\dot{m}_d$ was increased from a quiescent state with an e-folding time of ~ 2 days, while in the other case (using TCAFM3), the X_K was reduced exponentially at a similar rate.

The qualitative agreements clearly suggest that a series of quasi-steady two component solutions can explain the time variation of the spectral evolution of the X-ray novae. There is some underestimation of the hard X-rays for GS 1124-68 nova. This should disappear when more rigorous fitting routines capable of varying X_K and the central mass are used.

5. CONCLUDING REMARKS

In the present paper, we have made a thorough study of the spectral properties of two component accretion disk models. We considered the spectral variation when individual rates are changed, and also when the location (X_K) where the flow deviates from a Keplerian disk is varied. All possible configurations of the sub-Keplerian flow, including strong and weak shocks, no-shocks and the flow without angular momentum are taken into account as dictated by actual solutions of the governing equations. Generally speaking, we find that such a model is capable of explaining most, if not all, of the observational features of the black hole candidates. Particularly important is the fact that the models are based on the solid foundation of being constructed out of theoretical solutions of black hole accretion, rather than assuming ad hoc components (as in

models with static gaseous [e.g., Haardt & Maraschi, 1991] or magnetic [e.g., Galeev, Viana & Rosner, 1979] corona). The enhanced density region of the sub-Keplerian flow outside the horizon adequately serves as the so-called Compton cloud which has eluded astrophysicists for the past two decades. The oscillation of the post-shock region similarly produces quasi-periodic oscillations as observed in black hole candidates (Molteni, Sponholz & Chakrabarti, 1995; Ryu, Chakrabarti & Molteni, 1996 and references therein). The detailed properties of the multiwavelength novae light curves also come out very naturally from our model.

Whereas a single component, axisymmetric, transonic flow has been tested sufficiently well for stability (Chakrabarti & Molteni, 1995; Ryu, Chakrabarti & Molteni, 1996), the two component models presented here have not been adequately tested. This question is important because two flows of different viscosities may give rise to some instabilities at the interface, although the effect may be minimized due to the presence of mainly *supersonic* sub-Keplerian flow above and below the generally sub-sonic Keplerian disk. Efforts are being made to perform fully consistent numerical simulations, and the results should be reported in the near future.

The author thanks Drs. S. Kitamoto, K. Ebisawa and L. Titarchuk for discussions. He is also grateful to the referee, Prof. Paul Wiita for reading the manuscript very carefully and suggesting improvements.

REFERENCES

Cannizzo, J.K., 1993 in *Accretion Disks in Compact Stellar Systems*, ed. J. Craig Wheeler (Singapore: World Scientific), 6

Chakrabarti, S.K., 1989, ApJ, 347, 365 (C89)

Chakrabarti, S.K. 1990, Theory of Transonic Astrophysical Flows (Singapore: World Sci.) (C90)

Chakrabarti, S. K., 1996a, ApJ, 464, 664 (C96a)

Chakrabarti, S.K. 1996b, in Accretion Processes on Black Holes, Physics Reports, v. 266, No. 5 & 6, p 229 (C96b)

Chakrabarti, S.K., 1996c, MNRAS, 283, 325

Chakrabarti, S.K., 1997 in Accretion Phenomena and Related Outflows, eds. D. Wickramsinghe, L. Ferraro & G. Bicknell (in press).

Chakrabarti, S.K., & Molteni, D. 1995, MNRAS, 272, 80 (CM95)

Chakrabarti, S.K., & Titarchuk, L.G., 1995, ApJ, 455, 623 (CT95)

Chakrabarti, S.K., & Wiita, P.J. 1992, ApJ, 387, L21

Ebisawa, K. et al. 1994, PASJ, 46, 375 (E94)

Ebisawa, K., Titarchuk, L. & Chakrabarti, S.K. 1996, PASJ, 48, 1

Galeev, A. A, Rosner, R., & Viana, G. S. 1979, ApJ, 219, 318

Haardt, F. & Maraschi, L. 1991, ApJ, 411, L95

Kazanas, D., Hua, X.M. & Titarchuk, L.G. ApJ(in press)

Kitamoto, S. et al. 1992, ApJ, 394, 609

Molteni, D., Sponholz, H. & Chakrabarti, S.K. 1996 ApJ, 457, 805

Paczyński, B., & Wiita, P.J., 1980, A&A, 88, 23.

Ryu, D., Chakrabarti, S. K., & Molteni, D. 1997, ApJ(in press).

Shakura, N. I. & Sunyaev, R. A. 1973, A&A, 24, 337

Shimura, T. & Takahara, F. 1995, ApJ, 445, 780

Sunyaev, R.A. & Titarchuk, L.G. 1985, A&A, 143 374 (ST85)

Tanaka, Y. 1991 in Iron Line Diagnostics in X-ray Sources A. Treves et al. Springer-Verlag: Heidelberg, 98

Titarchuk, L.G. 1994, ApJ, 434, 570 (T94)

Zhang, S.N. in Accretion Phenomena and Related Outflows, eds. D. Wickramsinghe, L. Ferraro & G. Bicknell (in press).

FIGURE CAPTIONS

Fig. 1 Classification of the parameter space spanned by the specific energy $\mathcal{E}$ and angular momentum l for a thin, inviscid, flow in Schwarzschild geometry. Regions SA and SW produce standing shocks in accretions and winds respectively. See text for details.

Fig. 2 Schematic diagram of a multi-component accretion flow. Keplerian disk (cross-hatched) is flanked by (a generally) quasi-spherical sub-Keplerian halo which produces a centrifugal pressure supported hot dense region around the compact object. In the hard state, X_{K2}, the Keplerian disk becomes sub-Keplerian and produces a giant torus of about $10^4 R_g$, which collapses as viscosity is increased and the object goes to soft state. When the shock is absent $X_S \sim X_{K1}$ becomes the centerifugally supported dense region which reprocesses soft photons in the same way as the post-shock flow.

Fig. 3 Spectral evolution of an accretion disk with a strong shock (Model TCAFM1) at $X_s = 10$ around a black hole of mass $3.6 M_\odot$. The sub-Keplerian halo rate is $\dot{m}_h = 1$ and the Keplerian rates are marked on the curves. The dotted curve is drawn to include the effect of bulk motion Comptonization when $\dot{m}_d = 1$.

Fig. 4a-b (a) Spectral variation and (b) electron temperature variation (dotted curve) in the $\mathrm{TCAFM1}_2$ model where the sum of the disk and the halo rate is kept constant. In (a), we also include the bulk motion Comptonization when $\dot{m}_d = 1.5$ and in (b) we include the electron Temperature variation in TCAFM1 (Fig. 3) for comparison (solid curve). In $\mathrm{TCAFM1}_2$, electron temperature in hard states remains constant to a greater extent before catastrophically becoming too small in the soft state.

Fig. 5 Spectral variation with the Keplerian disk accretion rate $\dot{m}_d$ (as marked) while the halo rate $\dot{m}_h$ is chosen to be unity as before. The result is from the TCAFM3 model where the sub-Keplerian halo is devoid of angular momentum and therefore has no centrifugal barrier. Soft states are achieved even when the accretion disk rate is very low (compare with Fig. 3 and Fig. 4a above).

This preprint was prepared with the AAS LaTeX macros v4.0.

Fig. 6a-b (a) Spectral variation of TCAFM3 when X_K is monotonically decreased from 400 to 10; the curves are drawn for X_K = 400, 350, 300, 260, 230, 200, 170, 140, 120, 100, 100, 90, 50, 30, 20, and 10 respectively. The corresponding variation in spectral index is shown in (b). The greater interception of soft photons causes the black hole to go from the hard state to the soft state. Here, the fixed rates are: $\dot{m}_h = 1$, $\dot{m}_d = 0.05$.

Fig. 7a-b Similar to Fig. 6a, but X_K (marked on the curves) could be very far away as in a low accretion rate disk. $\dot{m}_h = 1.0$ and $\dot{m}_d = 0.001$ in (a) and 0.01 in (b). In (a), disk becomes very bright in hard states before becoming fainter (though remaining hard), while in (b), disk becomes very bright as X_K is decreased but subsequently becomes faint as it reached the soft state when $X_K \sim 30$.

Fig. 8 Spectral variation in TCAFM2. In this case the shock is very weak or absent but the centrifugal barrier causes the density enhancement close to the black hole exactly same as in a shocked flow (albeit gradually); $\dot{m}_h = 1$ and $\dot{m}_d$ are as marked. Hard to soft state transitions take place due to increase in the number of soft photons relative to the electron numbers as in TCAFM1 (Fig. 3).

Fig. 9 Spectral variation in TCAFM2$_2$ model with X_K marked on the curves. $\dot{m}_h = 1.0$ and $\dot{m}_d = 0.01$. For very high X_K the hard X-ray intensity is brightest. As viscosity of the flow is increased, and X_K decreases, the object goes to the soft-state.

Fig. 10a-b (a) Spectral variation in SCAFM$_2$. Here a single component Keplerian disk goes completely sub-Keplerian so that $\dot{m}_h \sim 0$. $\dot{m}_d = 0.01$ is chosen. X_K values are as marked. Here one always has a soft-component. Bulk motion Comptonization is neglected. In (b), we compare spectral index of this model (long dashed) with those of TCAFM2$_2$ (solid curves) and TCAFM3$_2$ (dotted curves) as functions of X_K, the location where the flow deviates from a Keplerian disk.

Fig. 11a-b Model dependence of spectral properties. (a) Solid, long-dashed and short-dashed curves are for TCAFM1, TCAFM2 and TCAFM3 respectively. (b) Spectral indices of the corresponding models as functions of $\dot{m}_d$. For comparison, included TCAFM1$_2$ model solutions (short-dash-dotted curves) are included, where the sum $\dot{m}$ of the rates is kept constant (2 for the upper curve and 1 for the lower curve). The variation of index due to bulk motion Comptonization is also included. The region $\dot{m}_d \sim 0.3-1$ may show break in spectral index as the effects of both the thermal Comptonization and bulk motion Comptonization would be present. The long-dash-dotted curve is also for bulk motion Comptonization but the presence of shock is assumed which enhances density in the flow for a given accretion rate.

Fig. 12a-d Qualitative fits of evolution of two X-ray novae spectra using two component accretion flow model (TCAFM1) and comparison of derived light curves with the observed light curves. See text for details.

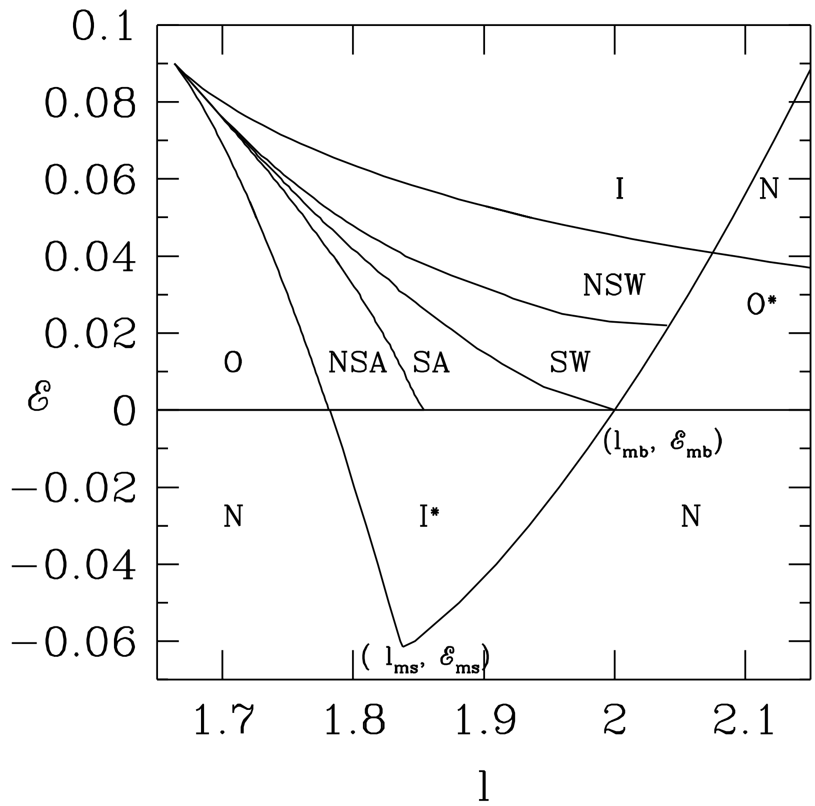

0.1
0.08
0.06
0.04
0.02
0
−0.02
−0.04
−0.06
ℰ
1.7
1.8
1.9
2
2.1
l
I
N
NSW
O*
O
NSA
SA
SW
(l_mb, ℰ_mb)
N
I*
N
(l_ms, ℰ_ms)

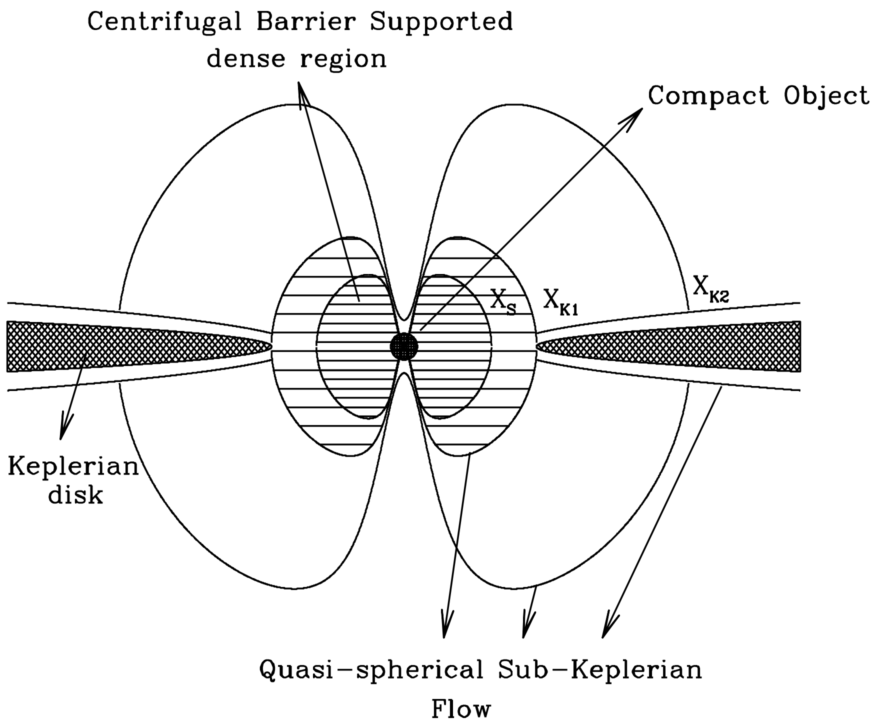

Centrifugal Barrier Supported
dense region
Compact Object
X_S
X_{K1}
X_{K2}
Keplerian
disk
Quasi−spherical Sub−Keplerian
Flow

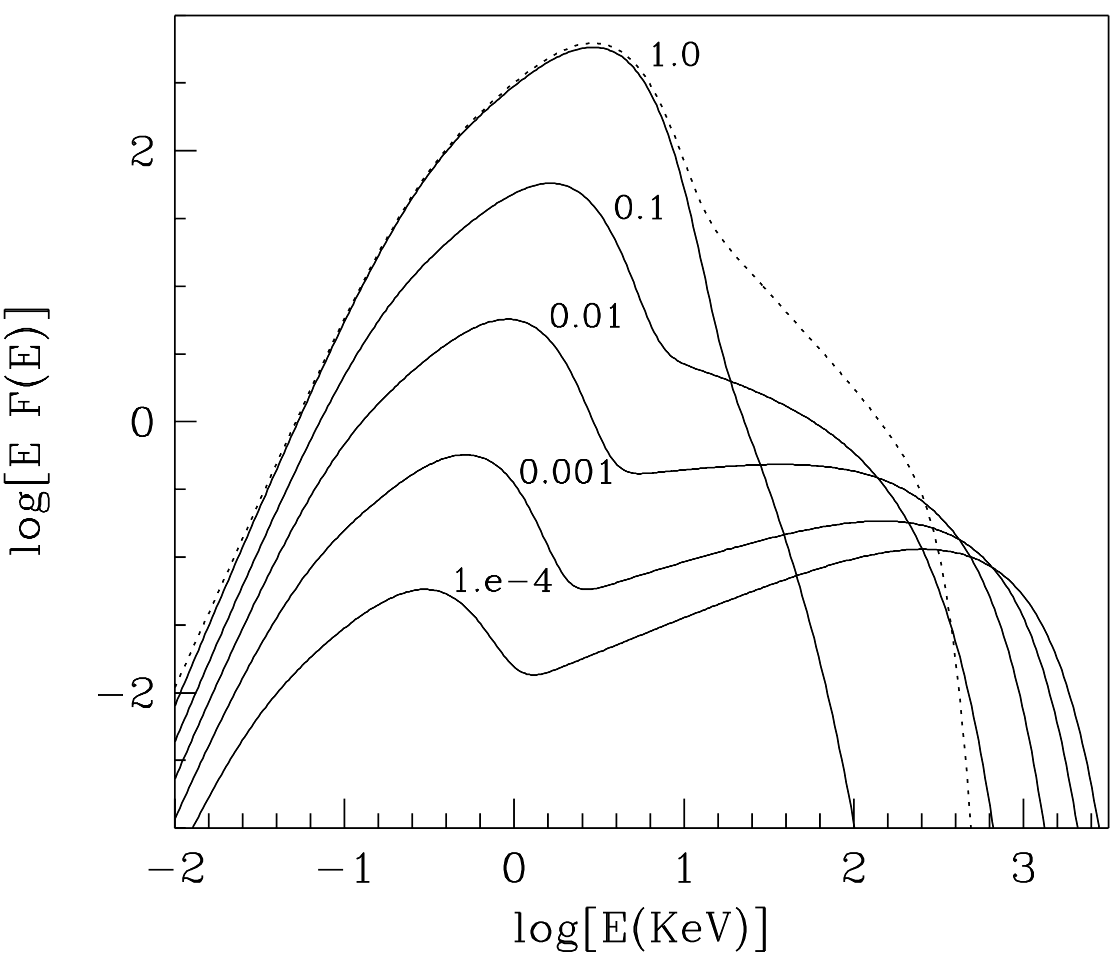

1.0
0.1
0.01
0.001
1.e−4
log[E F(E)]
log[E(KeV)]
−2
−1
0
1
2
3
2
0
−2

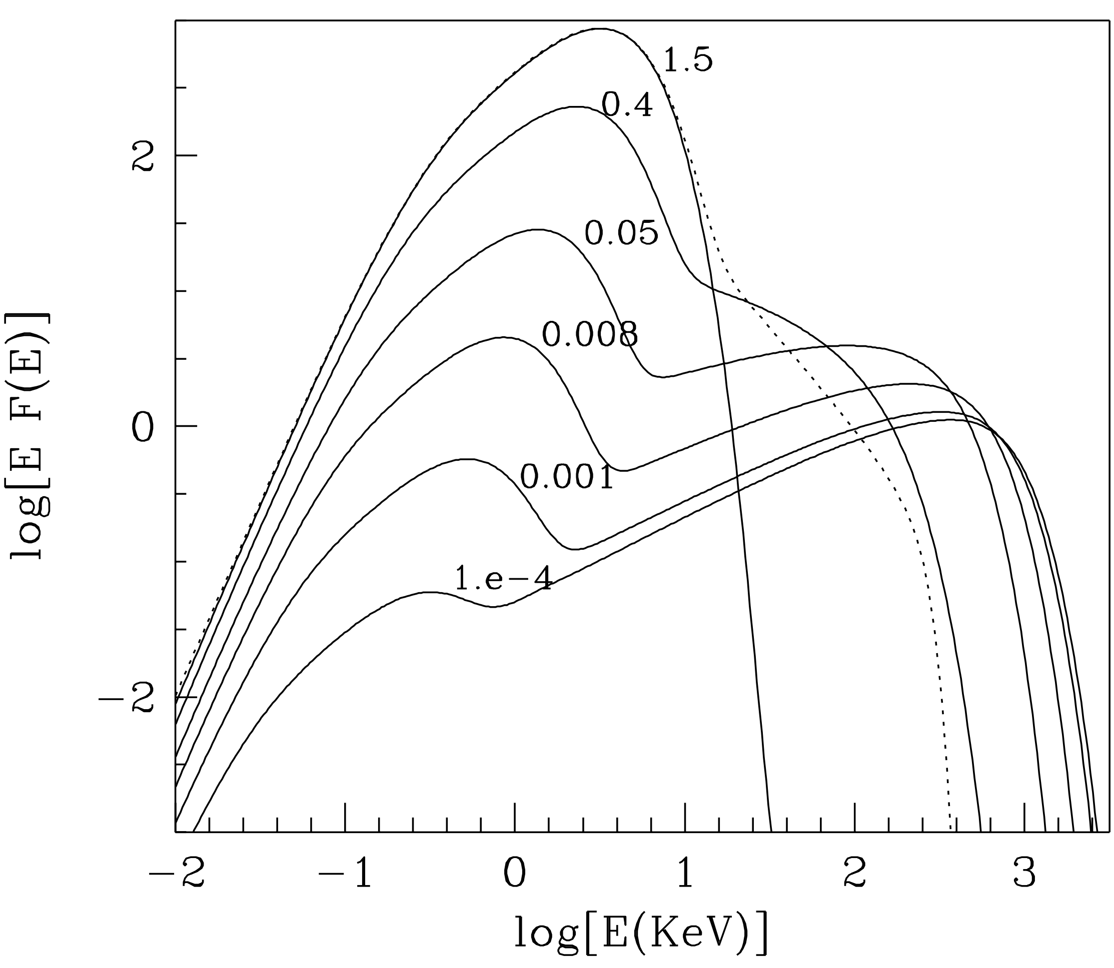

1.5
0.4
0.05
0.008
0.001
1.e−4
log[E F(E)]
log[E(KeV)]

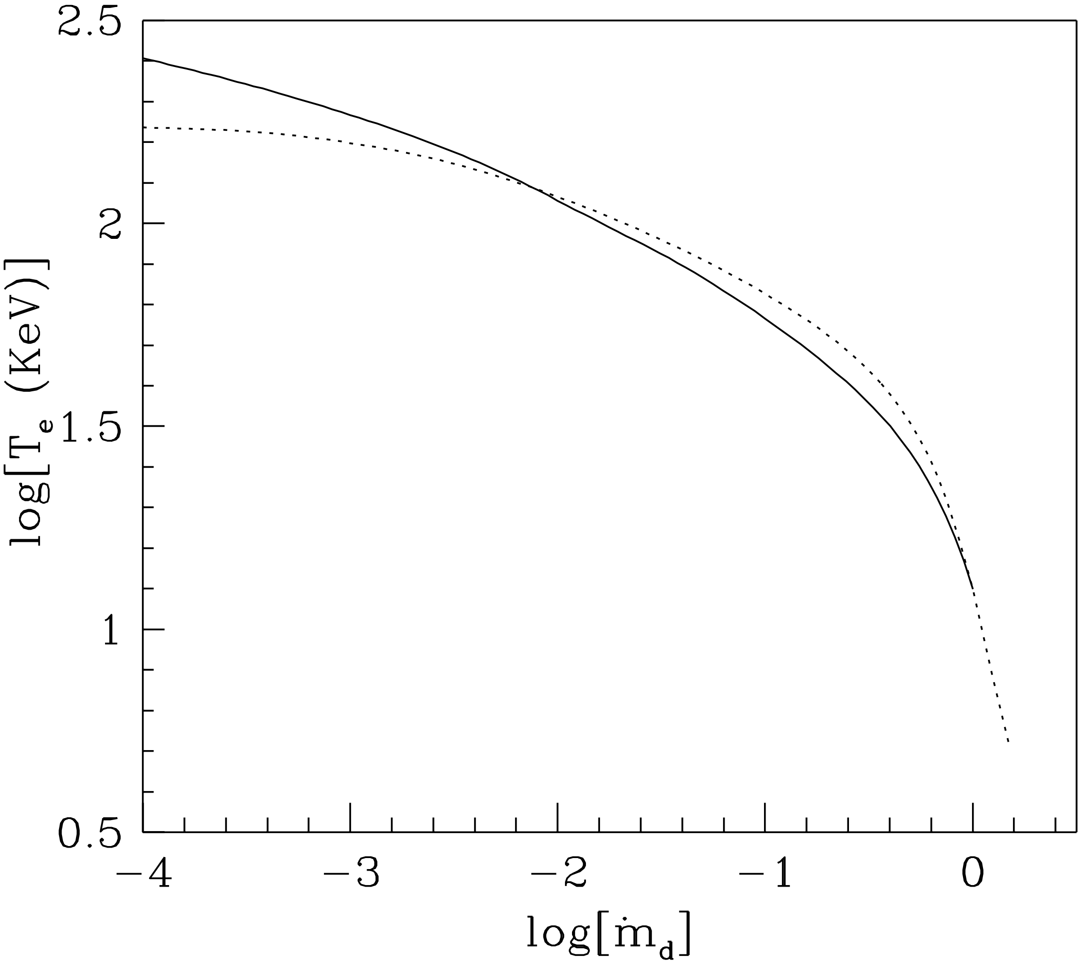

2.5
2
1.5
1
0.5
−4
−3
−2
−1
0
log[T_e (KeV)]
log[$\dot{m}_d$]

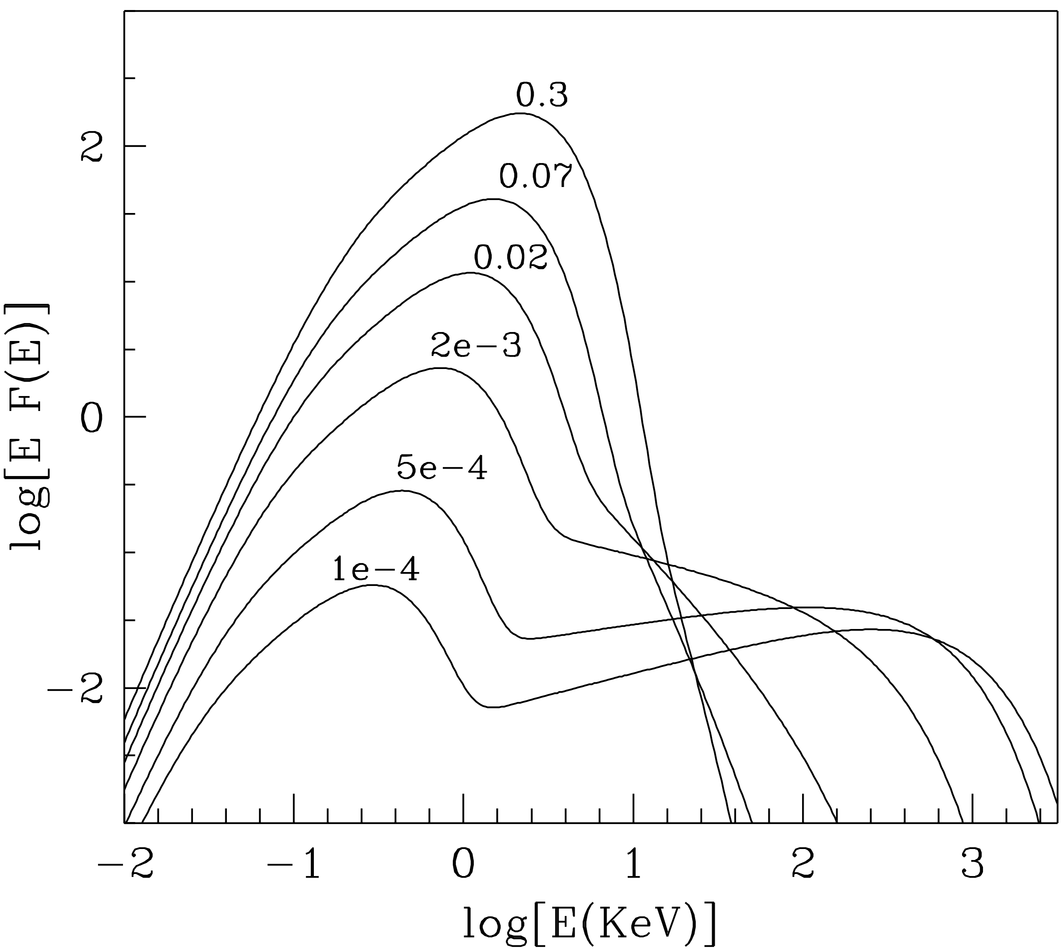

0.3
0.07
0.02
2e−3
5e−4
1e−4
log[E F(E)]
log[E(KeV)]
2
0
−2
−2
−1
0
1
2
3

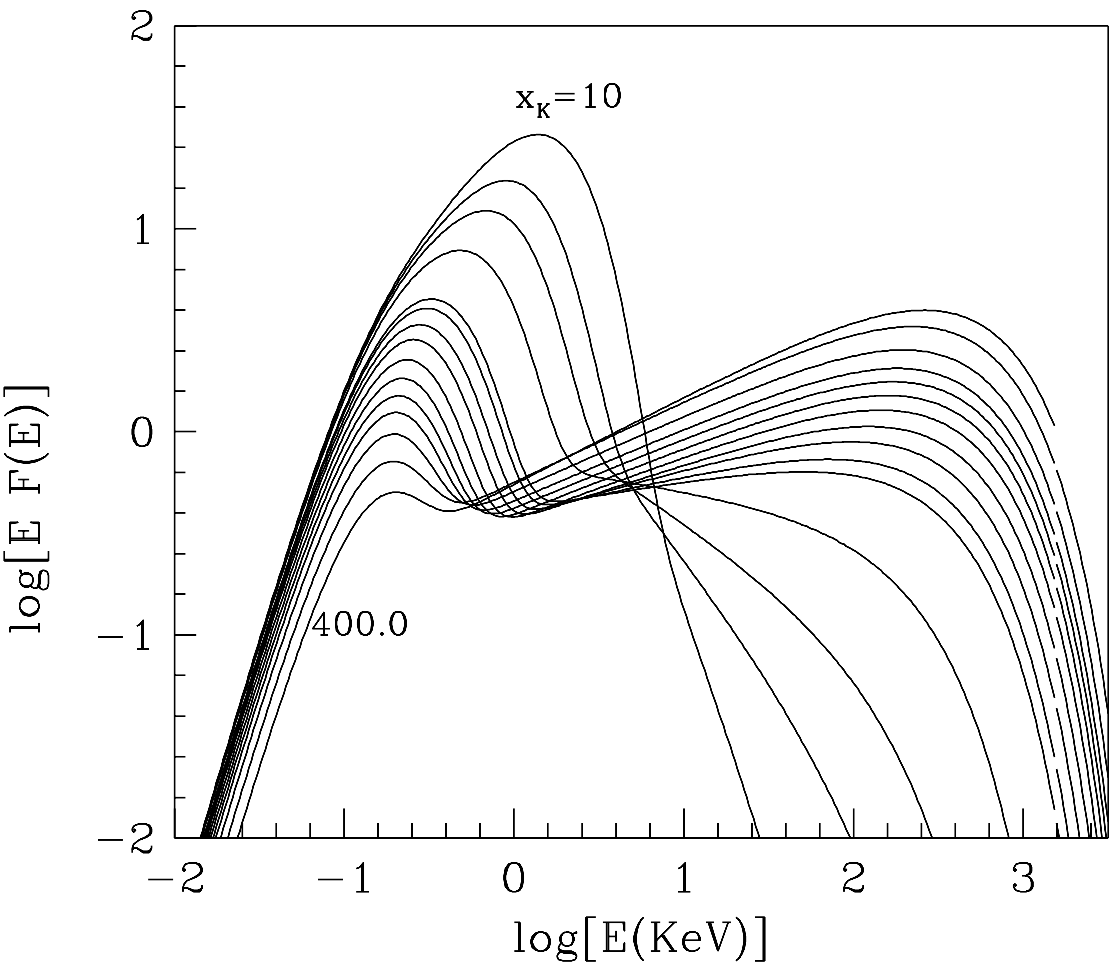

x_K=10
400.0
log[E F(E)]
log[E(KeV)]
2
1
0
−1
−2
−2
−1
0
1
2
3

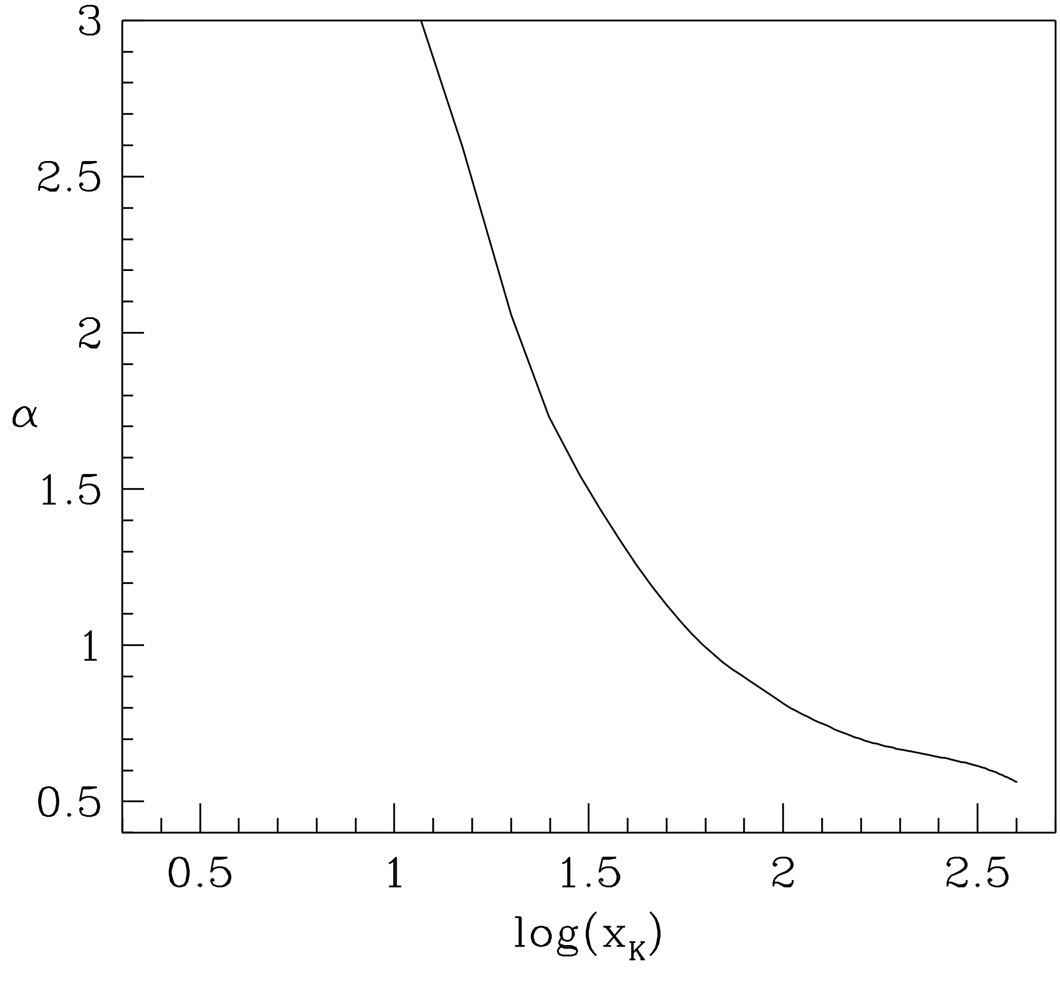

3
2.5
2
1.5
1
0.5
α
0.5
1
1.5
2
2.5
log(x_κ)

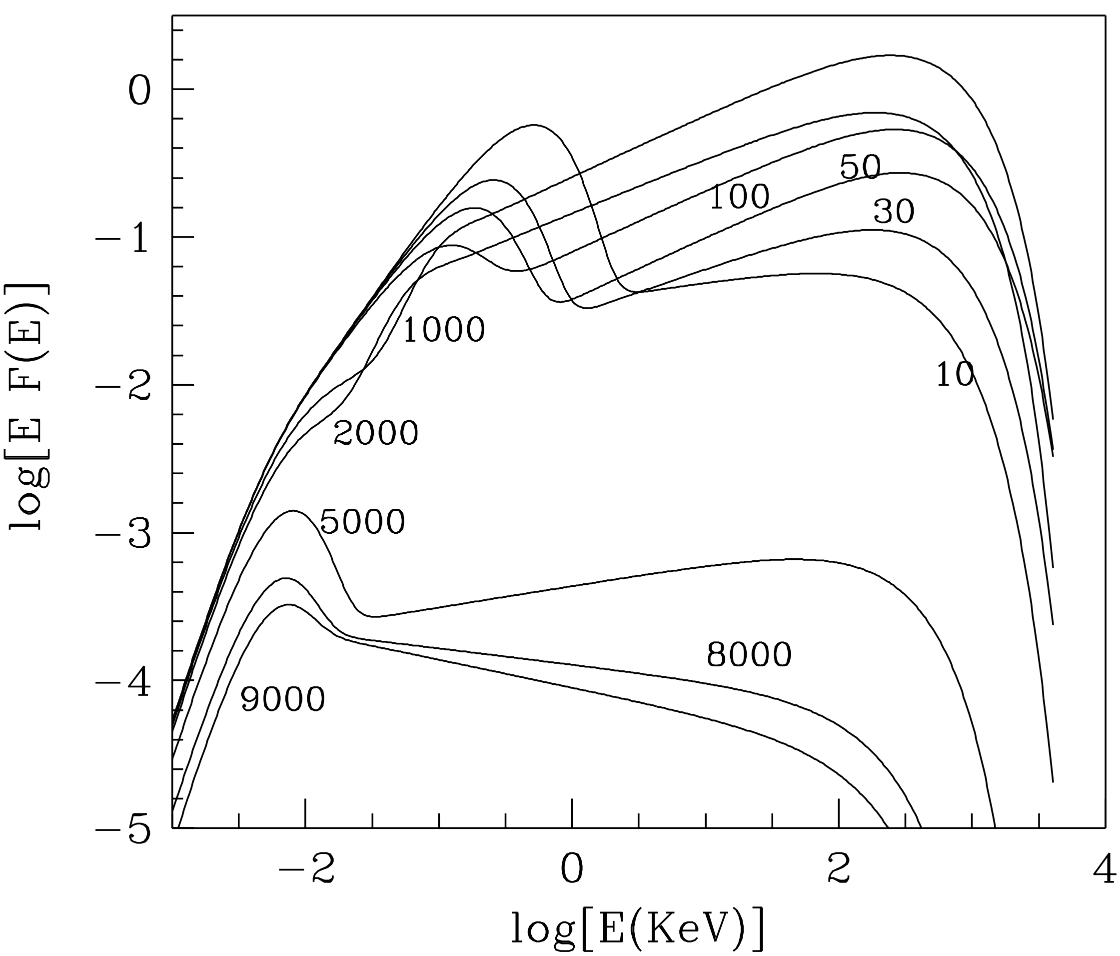

0
−1
−2
−3
−4
−5
log[E F(E)]
−2
0
2
4
log[E(KeV)]
50
100
30
10
1000
2000
5000
8000
9000

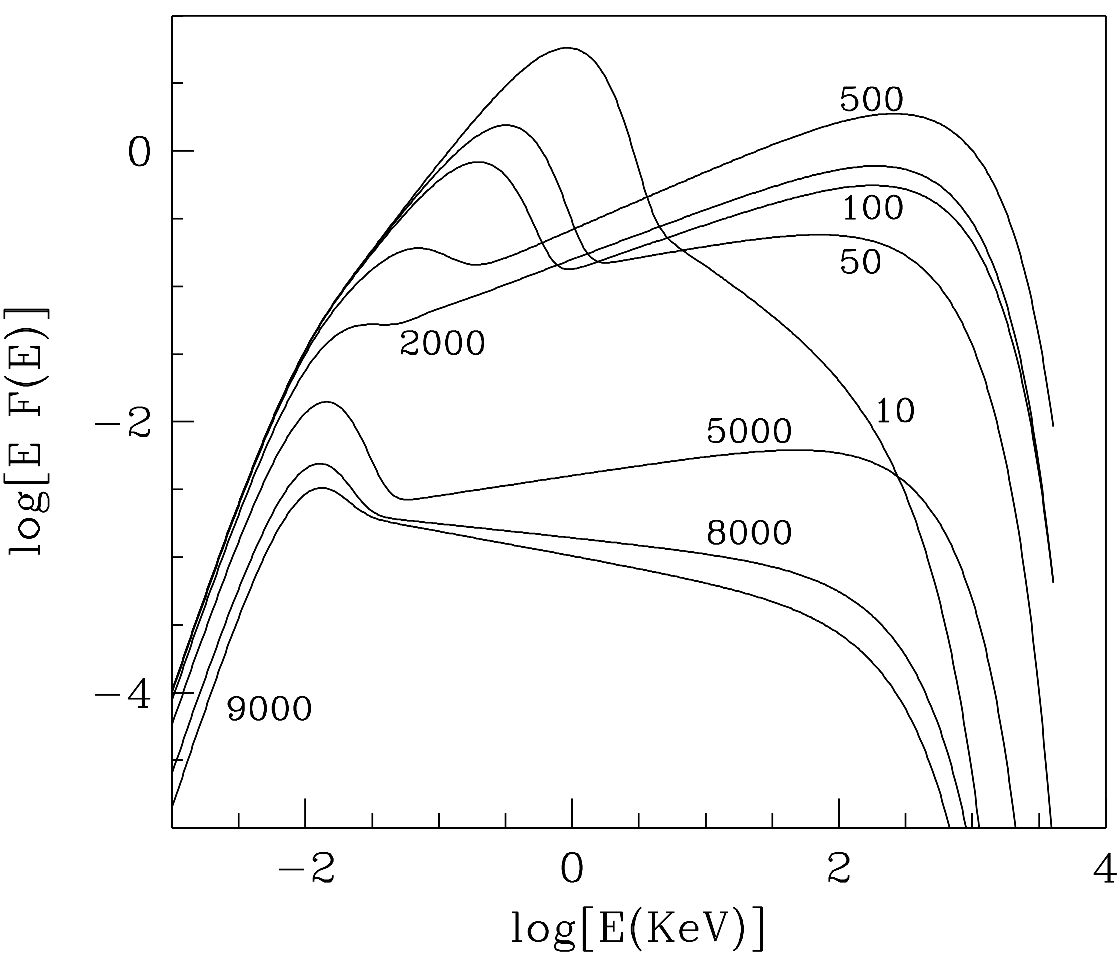

500
100
50
10
2000
5000
8000
9000
0
−2
−4
−2
0
2
4
log[E F(E)]
log[E(KeV)]

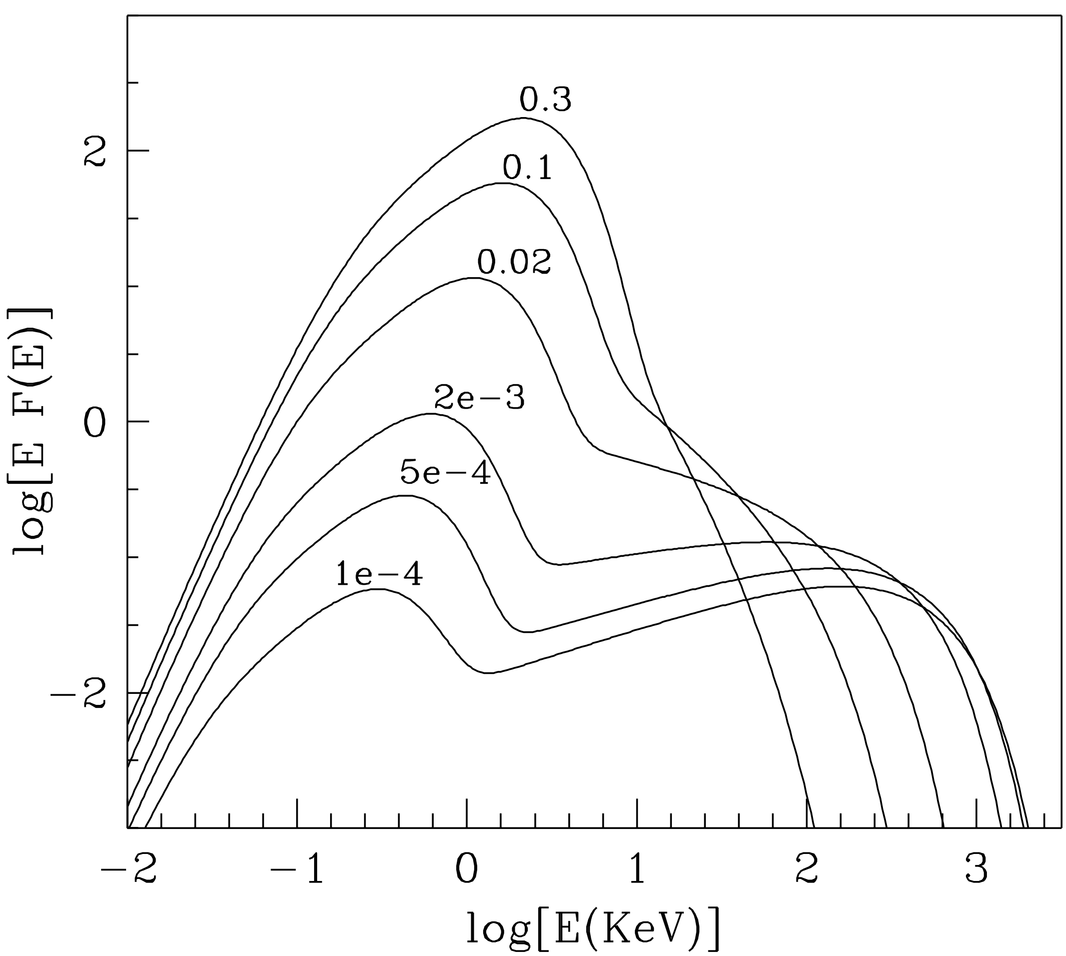

0.3
0.1
0.02
2e−3
5e−4
1e−4
2
0
−2
−2
−1
0
1
2
3
log[E F(E)]
log[E(KeV)]

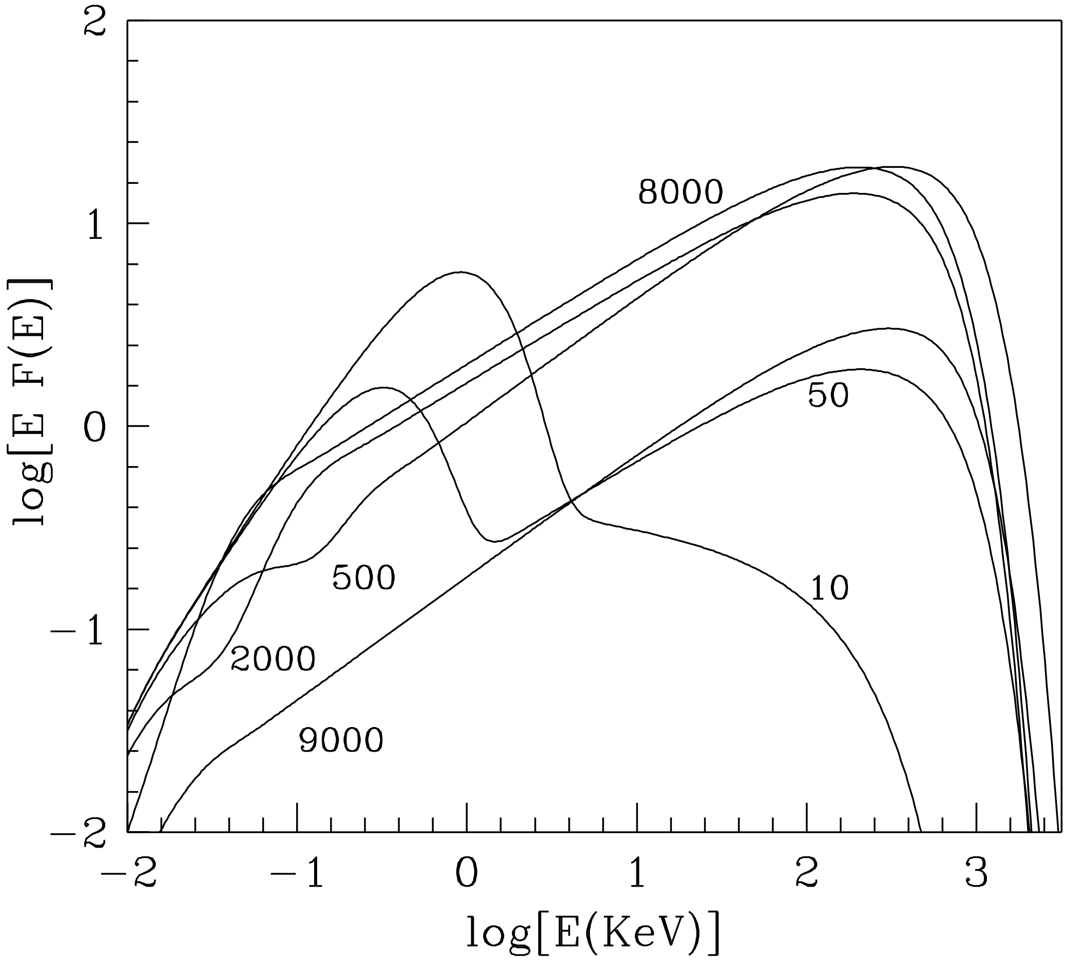

log[E F(E)]
log[E(KeV)]
2
1
0
−1
−2
−2
−1
0
1
2
3
8000
50
500
10
2000
9000

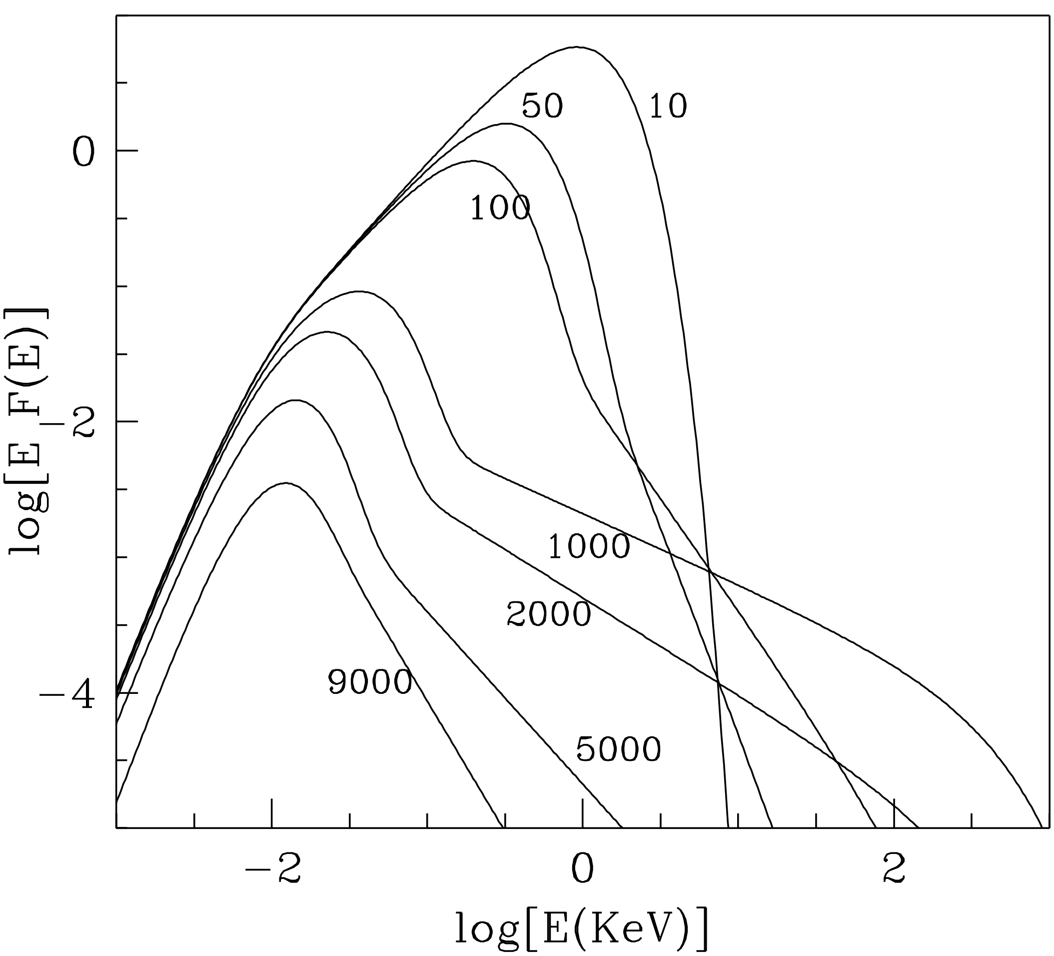

log[E F(E)]
log[E(KeV)]
10
50
100
1000
2000
5000
9000
0
−2
−4
−2
0
2

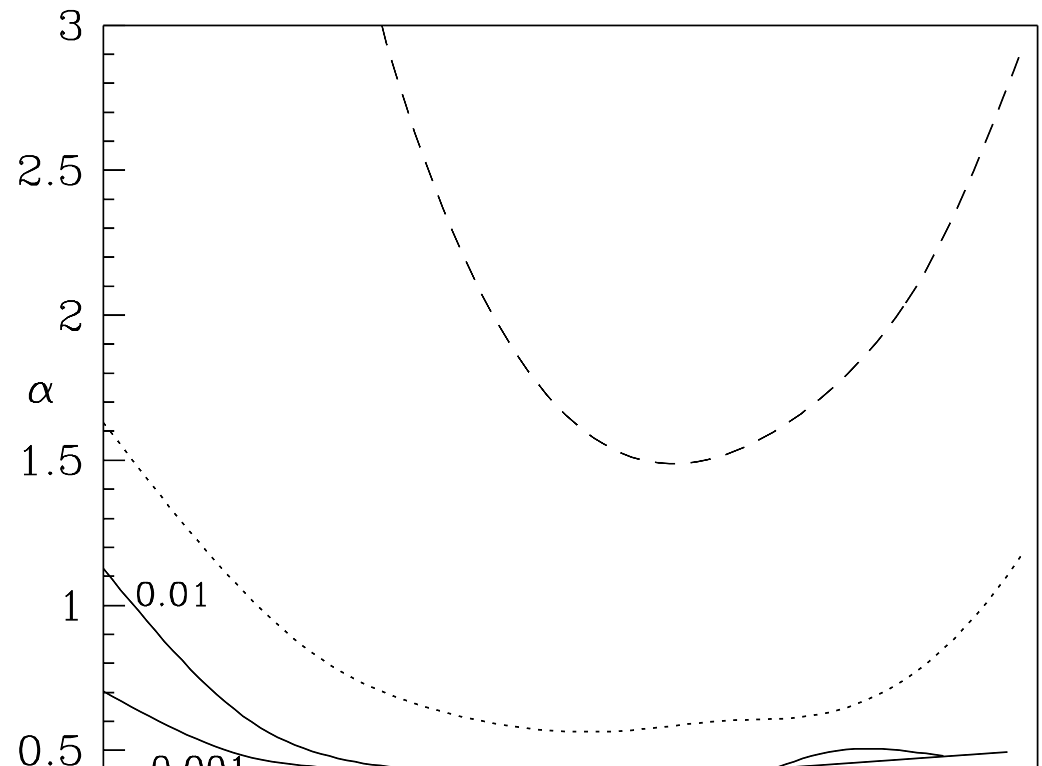

3
2.5
2
α
1.5
1
0.5
0.01
0.001
1
2
3
4
log(X_K)

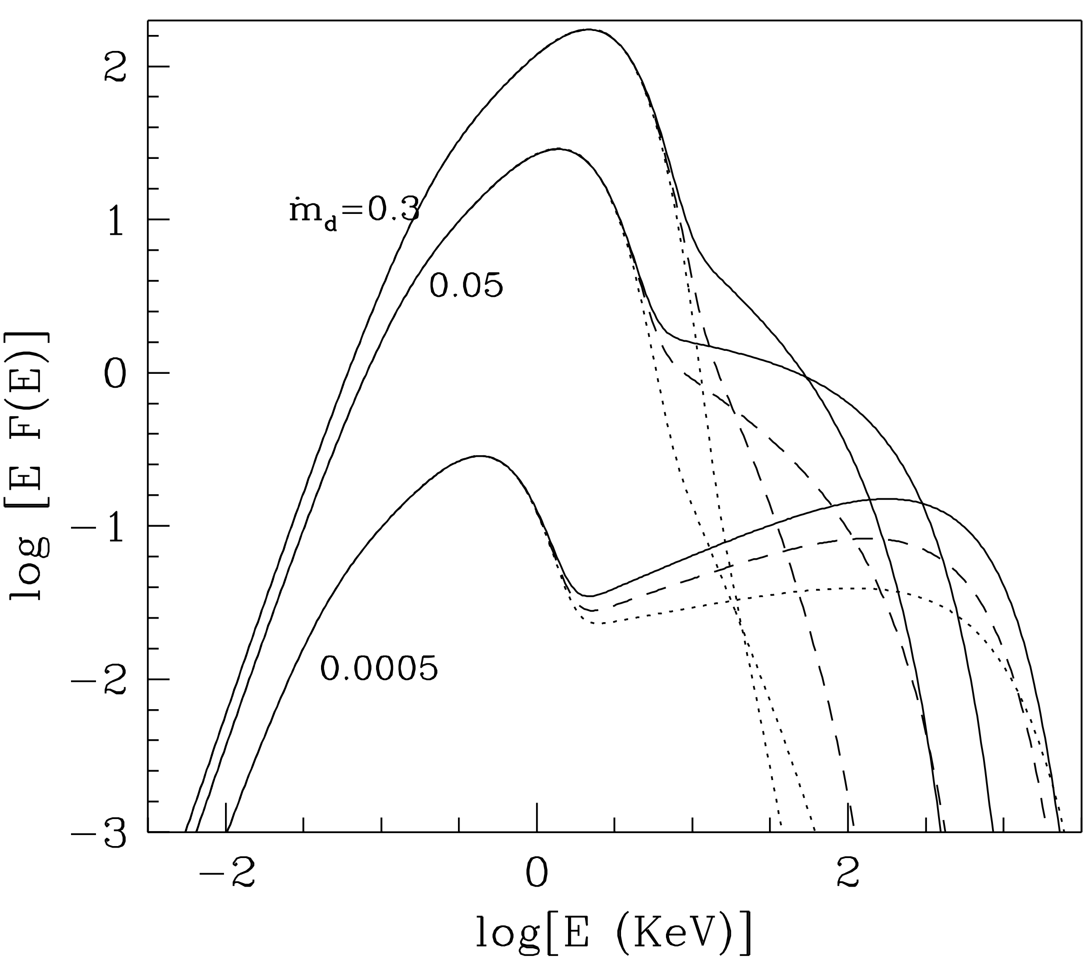

$\dot{m}_d$=0.3
0.05
0.0005
log [E F(E)]
log[E (KeV)]

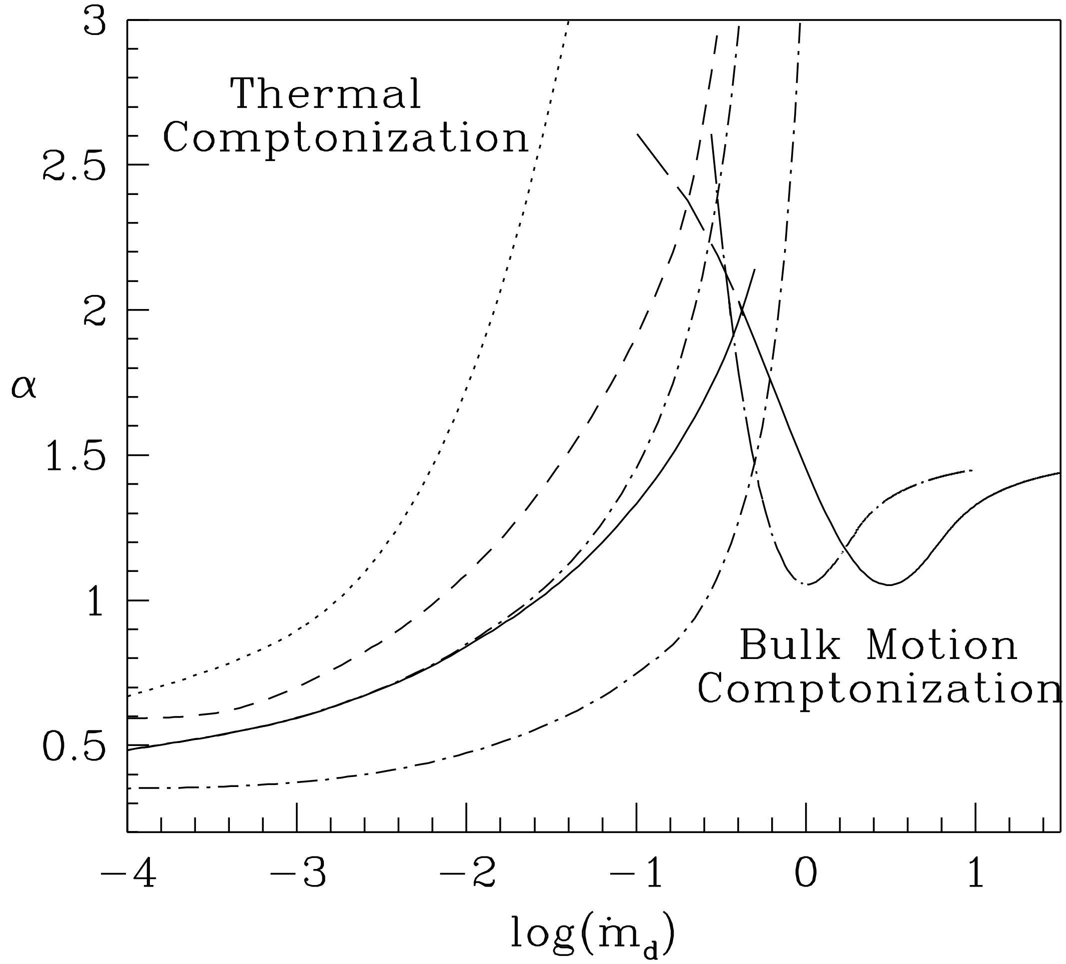

Thermal
Comptonization
Bulk Motion
Comptonization
α
log(ṁ_d)
3
2.5
2
1.5
1
0.5
−4
−3
−2
−1
0
1

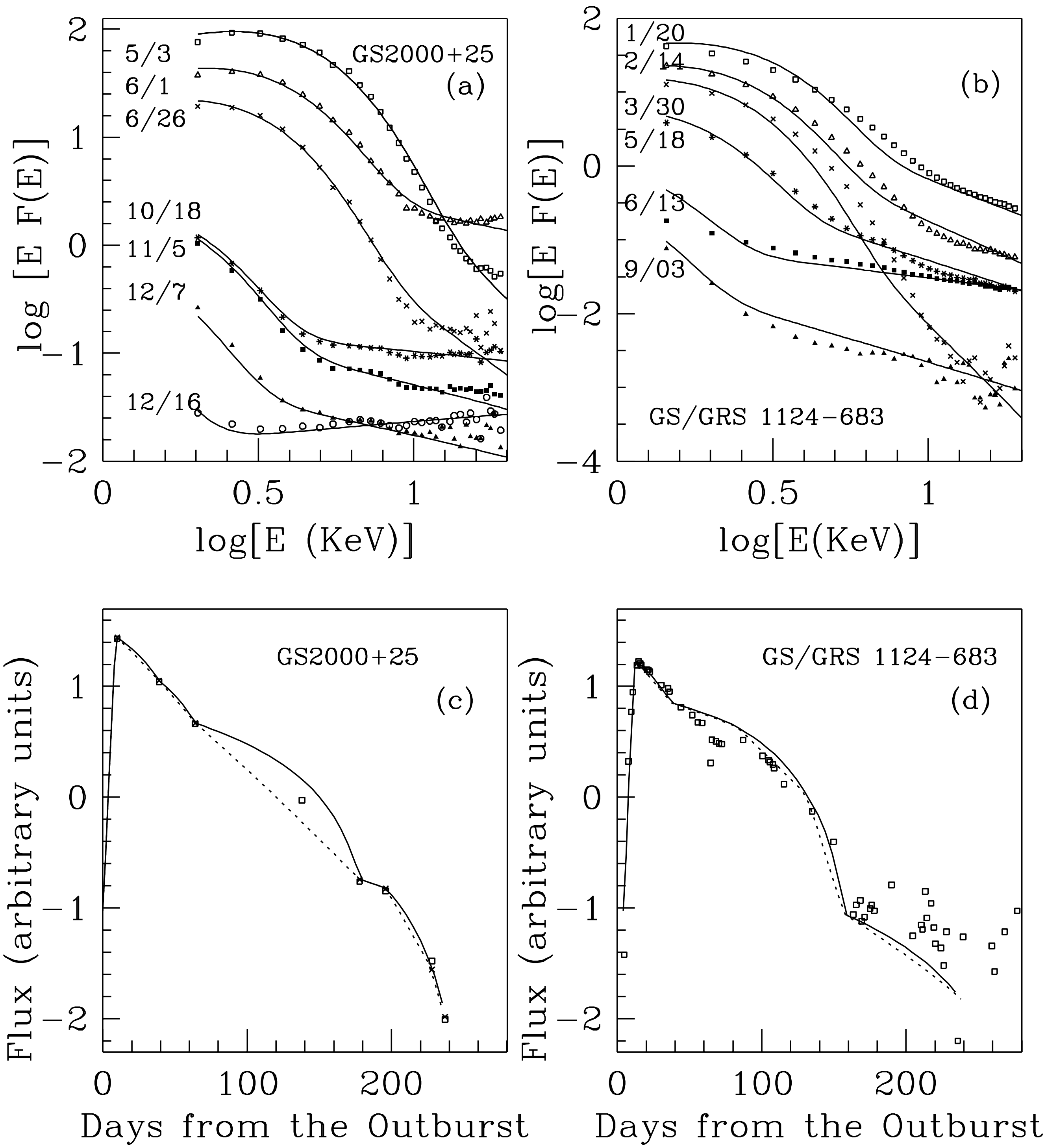
GS2000+25
(a)
5/3
6/1
6/26
10/18
11/5
12/7
12/16
log [E F(E)]
log[E (KeV)]
(b)
1/20
2/14
3/30
5/18
6/13
9/03
GS/GRS 1124-683
log [E F(E)]
log[E(KeV)]
GS2000+25
(c)
Flux (arbitrary units)
Days from the Outburst
GS/GRS 1124-683
(d)
Flux (arbitrary units)
Days from the Outburst